

Temperature-Sensitive Localized Surface Plasmon Resonance of α -NiS Nanoparticles


Published as part of *The Journal of Physical Chemistry virtual special issue "Marie-Paule Pileni Festschrift"*.

Rasmus Himstedt, Dirk Baabe, Christoph Wesemann, Patrick Bessel, Dominik Hinrichs, Anja Schlosser, Nadja C. Bigall, and Dirk Dorfs*

 Cite This: *J. Phys. Chem. C* 2021, 125, 26635–26644

 Read Online

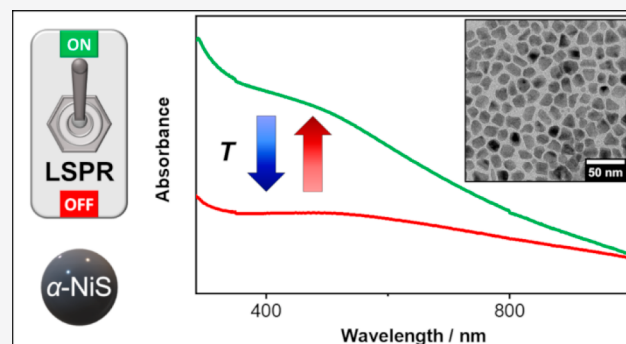
ACCESS |

 Metrics & More

 Article Recommendations

 Supporting Information

ABSTRACT: The presented work shows a synthesis route to obtain nanoparticles of the hexagonal α -NiS phase and core–shell particles where the same material is grown onto previously prepared Au seeds. In the bulk, this nickel sulfide phase is known to exhibit a metal–insulator type phase transition (MIT) at 265 K which drastically alters its electrical conductivity. Since the produced nanoparticles show a localized surface plasmon resonance (LSPR) in the visible range of the electromagnetic spectrum, the development of their optical properties depending on the temperature is investigated. This is the first time an LSPR of colloidal nanoparticles is monitored regarding such a transition. The results of UV–vis absorbance measurements show that the LSPR of the particles can be strongly and reversibly tuned by varying the temperature. It can be switched off by cooling the nanoparticles and switched on again by reheating them above the transition temperature. Additional to the phase transition, the temperature-dependent magnetic susceptibility of α -NiS and Au-NiS nanoparticles suggests the presence of different amounts of uncompensated magnetic moments in these compounds that possibly affect the optical properties and may cause the observed quantitative differences in the LSPR response of these materials.



INTRODUCTION

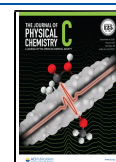
At room temperature, α -NiS (Ni_{1-x}S) is a metastable metallic nickel sulfide phase crystallizing in the hexagonal NiAs structure.¹ By cooling the material to temperatures below 260–270 K, a reversible first-order phase transition can be triggered.¹ Along with this transition, the electrical conductivity of the sample is drastically reduced (the specific resistivity changes from about 10^{-5} to 10^{-3} Ω cm), and the magnetism of the bulk material changes from paramagnetic to antiferromagnetic, whereas the structure of the hexagonal system is only slightly altered.² The a and c lattice parameters are increasing by 0.3 and 1%, respectively, while the volume of the unit cell increases by 1.3%.^{1,3} In contrast to most other metal–insulator transition materials (e.g., Ti_2O_3 , V_2O_3 , and VO_2),⁴ the low-temperature phase of α -NiS is not an electrical insulator or semiconductor but a poorly conducting metal instead.² Since the high-temperature phase is a well-conducting metal, nanoparticles of this material should show a localized surface plasmon resonance (LSPR). This has already been shown for different metallic nickel sulfide phases such as Ni_3S_2 and Ni_3S_4 .⁵ It is therefore interesting to investigate the LSPR of α -NiS nanoparticles and its dependence on the temperature. In this work, a synthesis to produce α -NiS as well as Au- α -NiS

(Au-NiS) core–shell nanoparticles is developed and the obtained particles are characterized in colloidal solution using temperature-dependent optical spectroscopy. In the case of α -NiS, only optical reflectivity measurements on the bulk material have been conducted so far.⁶ To the best of the authors' knowledge, an optical investigation of an LSPR in the visible regime of the electromagnetic spectrum in combination with a metal–insulator type transition or an analysis of a plasmonic material showing such a transition in colloidal solution has not been reported yet. The only other studies of this type, which were conducted very recently, were working with films of VO_2 particles with diameters larger than 70 nm, showing infrared LSPR signals.^{7–9}

Received: September 24, 2021

Revised: November 4, 2021

Published: November 23, 2021



METHODS

Materials. Hydrogen tetrachloroaurate trihydrate ($\text{HAuCl}_4 \cdot 3\text{H}_2\text{O}$, 99.99%) and nickel chloride hexahydrate ($\text{NiCl}_2 \cdot 6\text{H}_2\text{O}$, 99.9%) were obtained from abcr. Borane *tert*-butylamine complex (BBA, 97%), methanol (MeOH, 99.9%), and 1,2,3,4-tetrahydronaphthalene (97%) were obtained from Alfa Aesar. Acetone (99.7%), chloroform (99.8%), eicosane (99.5%), ethanol (EtOH, >98%), hydrochloric acid (HCl, 37%), nitric acid (HNO_3 , 69%), 1-octadecene (ODE, 90%), oleylamine (OLAm, 70%), thiobenzoic acid (TBA, 90%), and toluene (99.7%) were obtained from Sigma-Aldrich. Sodium carbonate (Na_2CO_3 , 98%) was purchased from VWR Chemicals.

Synthesis of Nickel Thiobenzoate (NiTB_2). The synthesis of NiTB_2 was done according to a previous study.¹⁰ Briefly, Na_2CO_3 (1.06 g) was dissolved in distilled water (20 mL) before TBA (2.35 mL) was added to the solution, which turned yellow and was stirred for 30 min afterward. Then $\text{NiCl}_2 \cdot 6\text{H}_2\text{O}$ (2.38 g) dissolved in distilled water (20 mL) was added to the reaction mixture, which was subsequently stirred for 60 additional min. The dark red product was precipitated by centrifugation (1 min, 3773g) and washed several times with distilled water and EtOH before it was dried under vacuum and finally stored under inert conditions.

Synthesis of α -NiS Nanoparticles. The synthesis was adapted and modified from a known procedure.¹¹ NiTB_2 (82 mg) was dissolved in OLAm (0.8 mL) by stirring at 40 °C for 2 h. The resulting solution was then injected into OLAm (4 mL), which was previously degassed under vacuum for 2 h at 100 °C, at 200 °C under an Ar flow. After 1 min of reaction time, the mixture was cooled down and toluene (5 mL) was injected. The nanoparticles were precipitated once via the addition of MeOH (5 mL) and subsequent centrifugation (10 min, 3773g). They were then redispersed and stored in toluene (8 mL). The whole process was conducted under inert conditions.

Synthesis of Small Au Nanocrystals (AuNCs). The synthesis of small quasi-spherical gold nanocrystals was carried out via the reduction of tetrachloroaurate in the presence of OLAm.¹² $\text{HAuCl}_4 \cdot 3\text{H}_2\text{O}$ (0.2 g) was dissolved in a mixture of 1,2,3,4-tetrahydronaphthalene (10 mL) and OLAm (10 mL). The solution was cooled to 0 °C. A freshly prepared solution of BBA (87 mg) in 1,2,3,4-tetrahydronaphthalene (1 mL) and OLAm (1 mL) was injected into the reaction mixture. The solution was stirred for two additional hours. Afterward, the AuNCs were precipitated by the addition of acetone (\approx 140 mL), centrifuged (5 min, 5000g), and dispersed in toluene. This cleaning step was repeated. Finally, the product was redispersed and stored in toluene. The average diameter of the AuNCs in the obtained highly monodisperse samples varies from batch to batch and usually lies between 4 and 6 nm. Smaller AuNCs can be produced using increased reaction temperatures (e.g., 40 °C for diameters <3 nm).

Synthesis of Large AuNCs (>6 nm). For the preparation of larger AuNCs, a seed-mediated growth approach was used and modified.¹³ For the synthesis of 10 nm gold nanocrystals, a solution of previously prepared AuNCs (\approx 6 nm diameter, 30 mg) was dispersed in a solution of $\text{HAuCl}_4 \cdot 3\text{H}_2\text{O}$ (100 mg) in ODE (10 mL) and OLAm (10 mL). The temperature was increased to 80 °C within 10 min and was held for an additional two hours. The product was precipitated by the addition of acetone, centrifuged (5 min, 5000g), and dispersed in toluene. This solution was used for a consecutive second

growing step in $\text{HAuCl}_4 \cdot 3\text{H}_2\text{O}$ (320 mg) in ODE (27 mL) and OLAm (27 mL). After cleaning via precipitation with acetone and centrifugation (5 min, 5000g), the particles were collected in toluene. For the preparation of AuNCs with different diameters, the amount of gold precursor and/or the number of growing steps can be varied.

Synthesis of Au-NiS Core-Shell Particles (Exemplary Amounts for 6.1 nm Cores with a 4.6 nm Shell). The solvent of the AuNC dispersion (600 μL , particle concentration: 6.8×10^{-7} mol/L) was evaporated, the nanoparticles were redispersed in toluene (100 μL) and OLAm (0.5 mL), and the resulting solution was transferred into a syringe. Meanwhile, NiTB_2 (15 mg) was dissolved in OLAm (250 μL) by stirring at 40 °C for 2 h. This mixture was filled into a second syringe. Then, the content of the first syringe was injected into OLAm (4 mL), which was previously degassed under vacuum for 2 h at 100 °C, at 150 °C under an Ar flow. Subsequently, the solution inside the second syringe was added to the reaction mixture in a dropwise manner. After 1 min of further reaction time, the solution was cooled down and toluene (5 mL) was added. The product was precipitated via the addition of MeOH (5 mL) and centrifugation (10 min, 3773g) and finally redispersed and kept in toluene (8 mL). All steps during the synthesis were done under inert conditions. The thickness of the shell can be tuned by varying the amount of the seed particles or the NiTB_2 depending on the diameter of the chosen core nanocrystals.

Electron Microscopy. Transmission electron microscopy (TEM) measurements were conducted using a FEI Tecnai G2 F20 employing a field emission gun operated at 200 kV. The nanoparticles were cleaned by precipitation with methanol and redispersion in chloroform. The resulting solution was then drop-casted onto carbon-coated copper grids (300 mesh) by Quantifoil.

Elemental Analysis. The gold and nickel mass concentrations of the particle dispersions were determined via atomic absorption spectroscopy (AAS) using a Varian AA 140 spectrometer. Aliquots of the stable dispersions were taken, the solvent was evaporated, and the resulting residue was dissolved in aqua regia. The resulting solution was diluted with deionized water, and the atomic absorption was measured and related to the values of separately prepared calibration solutions with known Au or Ni mass concentrations. In the case of the Au-NiS nanoparticles, only the Ni mass concentration was used since the presence of Ni disturbs the measurement of Au with this device.

Optical Spectroscopy. For the acquisition of optical absorbance spectra, a Cary 5000 UV-vis/NIR spectrophotometer by Agilent Technologies was used in transmission mode. The sample dispersions were diluted with additional toluene and measured in high-performance quartz glass cuvettes with a path length of 1 cm by Hellma Analytics. In the case of the low-temperature measurements, a cryostat OptistatCF by Oxford Instruments was mounted into the device to enable the necessary temperature control via cooling with liquid nitrogen. After reaching each measurement temperature, a waiting time of 10 min was implemented in order to obtain a stable temperature in the cuvette. The dispersions were kept under an inert atmosphere during the whole process.

SQUID Magnetometry. Solid-state magnetic susceptibility measurements on polycrystalline powders of α -NiS and Au-NiS nanoparticles were performed on a Cryogenic Ltd. closed-

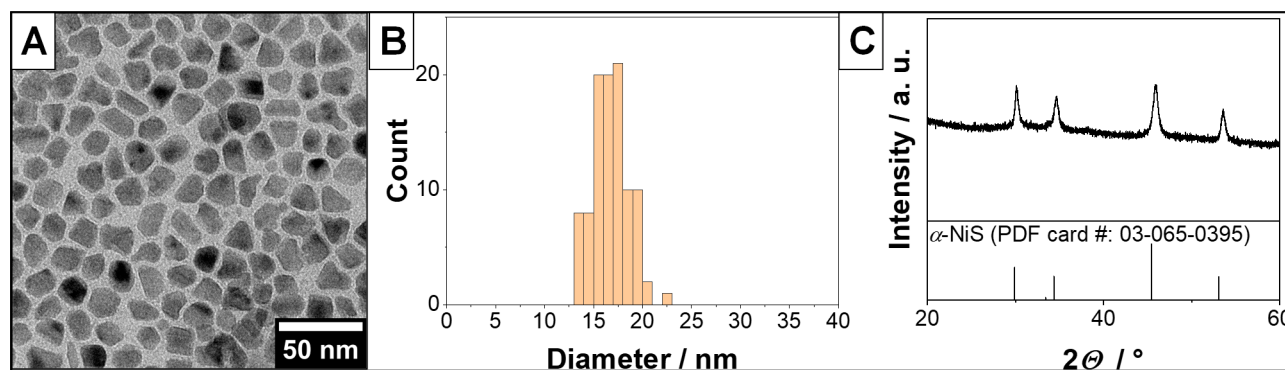


Figure 1. TEM overview image (A) of an exemplary sample of α -NiS nanoparticles and the corresponding size distribution (B). The average diameter of the particles is $16.8 \text{ nm} \pm 1.8 \text{ nm}$. (C) X-ray diffraction pattern of the same sample. The obtained crystal phase is hexagonal NiS (α -NiS, PDF card no. 03-065-0395) with no observable impurities.

cycle SQUID magnetometer at temperatures between $T = 4$ and 300 K with external magnetic fields of $H_{\text{ext}} = 1$ and 5 kOe. The measurements were executed with a field warming sequence starting at $T = 4$ K after zero-field or field cooling to the base temperature. Additional isothermal magnetization measurements on both compounds with external magnetic fields up to $H_{\text{ext}} = 70$ kOe were also executed at selected temperatures. The samples were prepared in gelatin capsules (size 4) by Plano. Before and after the addition of the sample a droplet of Eicosan (~ 10 mg each) was filled into the capsules to prevent movement or orientation of the material in the magnetic field. The particle synthesis had to be scaled up drastically ($\times 7$ and $\times 10$ for the α -NiS and Au-NiS synthesis, respectively) in order to produce enough material for the measurements. To remove the organic ligands, the obtained nanoparticle dispersions were washed once by precipitating them with methanol and afterward redispersed in chloroform. The resulting solution was then added dropwise into the capsule, while the chloroform evaporated over time and was therefore removed from the sample. In this way, amounts of 21.9 and 18.6 mg of the α -NiS and Au-NiS sample could be deposited in the capsules, respectively. The Au-NiS sample contained approximately 17.3 mg of α -NiS and 1.3 mg of Au according to a combined AAS and TEM analysis. The diamagnetic background signal of a gelatin capsule including a droplet Eicosan (19.0 mg) and mounted in a straw was experimentally determined ($\chi_0 = -3.10 \times 10^{-8} \text{ emu G}^{-1}$) and subtracted from the raw magnetization data. The experimental data were further corrected for the overall diamagnetism of the investigated molecules using an approximation for this contribution, i.e., $\chi_D = -0.5M \times 10^{-6} \text{ cm}^3 \text{ mol}^{-1}$, with M describing the (unitless) molar mass of the given molecule.¹⁴

X-ray Diffraction (XRD). XRD measurements were performed with a Bruker D8 Advance device in reflection mode. It was operated at 40 kV and 40 mA using Cu K-alpha radiation. The sample preparation was done analogously to the preparation for the TEM measurements. The nanoparticle dispersions in chloroform were drop-casted onto single crystalline silicon sample holders.

RESULTS AND DISCUSSION

Nickel sulfide nanoparticles were synthesized from a single-source precursor (NiTB_2) in an organic medium (oleylamine), which also provided the surface ligands for the particles. Figure 1A shows an exemplary TEM overview image of the obtained nanocrystals. They have a quasi-spherical shape, which tends to

be somewhat elongated in one axis due to the hexagonal crystal structure of the nickel sulfide. The average diameter of the particles is $16.8 \text{ nm} \pm 1.8 \text{ nm}$, and the corresponding narrow size distribution is displayed in Figure 1B. To confirm that the correct nickel sulfide phase has been synthesized, XRD measurements were conducted. The results are shown in Figure 1C, and it is obvious that nanocrystals of the hexagonal α -NiS phase have been obtained.

Previous studies have shown that other nickel sulfide materials tend to easily grow onto gold seed particles to form core-shell nanostructures.^{5,15} Since gold nanoparticles shall be used as plasmonic reference material in this work and these kinds of plasmonic core-shell structures tend to have optical properties, which are dominated by the shell material,^{5,16} this was also tested in the case of α -NiS in order to diversify the used materials. Gold nanocrystals (AuNCs) of varying sizes were therefore synthesized. TEM overview images and absorbance spectra of these can be found in Figure S1 of the Supporting Information. Using the AuNCs as seed material, a method to grow Au-NiS core-shell structures was developed and resulted in the nanoparticles shown in Figure 2. It can be seen that core-shell nanoparticles with narrow size-distributions can be obtained for various different seed diameters. The thickness of the α -NiS shell can be readily controlled by changing the amount of NiTB_2 used in the synthesis. The XRD pattern in Figure 2E shows that both Au and α -NiS are present in the respective sample of large core-shell particles. In the case of the smaller nanoparticles, only Au could be found in the XRD analysis due to its larger scattering cross-section if any reflections could be detected at all. This is due to the small size of the nanocrystals and in line with the results of previous studies on nanoparticles of different nickel sulfide phases.^{5,17} The results of these XRD measurements and a general optical analysis of these samples can be found in Figures S2 and S3 of the Supporting Information, respectively.

In order to investigate the temperature-dependent optical properties of the successfully synthesized α -NiS nanostructures, UV-vis absorbance measurements of diluted samples in toluene were conducted using a cryostat to cool the dispersions down to 235 K, which is well below the transition temperature of bulk α -NiS (265 K).² Spectra at different temperatures during the cooling and subsequent reheating of the samples are shown in Figure 3. AuNCs were used as a plasmonic reference material (Figure 3A,B). It can be observed that with decreasing temperature, the absorbance of their LSPR maximum at 523 nm is rising, which is the expected outcome.¹⁸ Due to the

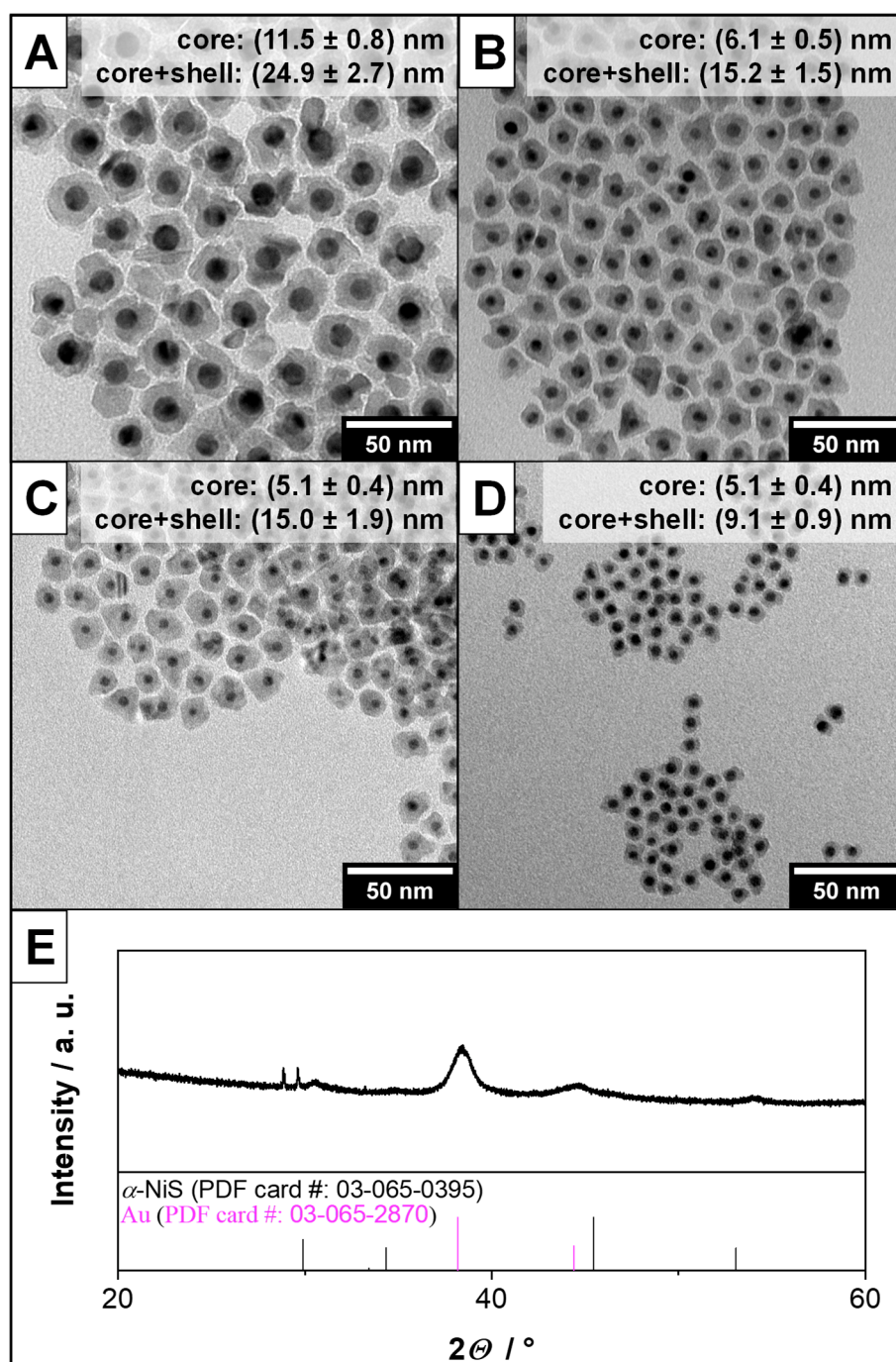


Figure 2. TEM overview image of different Au-NiS core-shell nanoparticle samples (A–D). It can be seen that the synthesis works using different core sizes and also that it is possible to tune the thickness of the α -NiS shell around the same Au cores (C and D). (E) XRD pattern of the sample depicted in part A. Reflections of the large gold cores can be observed as well as reflections that are attributed to the nickel sulfide shell.

smaller influence of lattice phonons at low temperatures (less electron–phonon scattering), the damping of the plasmon is weaker, which in turn leads to a more pronounced band in the absorbance spectrum.¹⁸ This process is reversible, and the original LSPR intensity is retained upon reheating the sample to room temperature. In the case of Au-NiS core-shell nanoparticles where the same AuNCs were used as seed particles for the growth of a 4.5 nm α -NiS shell (Figure 3C,D), the LSPR maximum is broader and hypsochromically shifted compared to the pure AuNCs. This can be explained by the fact that the plasmonic properties of the particles are dominated by the shell material, whose LSPR maximum is

located further toward the UV regime as it is also the case for a few other metallic nickel sulfide phases (cf., the spectra of pure α -NiS in Figure 3E,F).^{5,15} Upon cooling the Au-NiS sample, a similar behavior (i.e., a slight increase of the LSPR absorbance with decreasing temperature) is observed until a temperature below 250 K is reached. Then a sudden drop of absorbance at short wavelengths and an increase at long wavelengths are visible. This trend is also reversible upon reheating the dispersion, but the reversal of the change below 250 K happens here at higher temperatures. The 240 K spectrum is identical to the one taken at 250 K during reheating (this hysteresis will be investigated in Figure 4 in more detail). For pure α -NiS

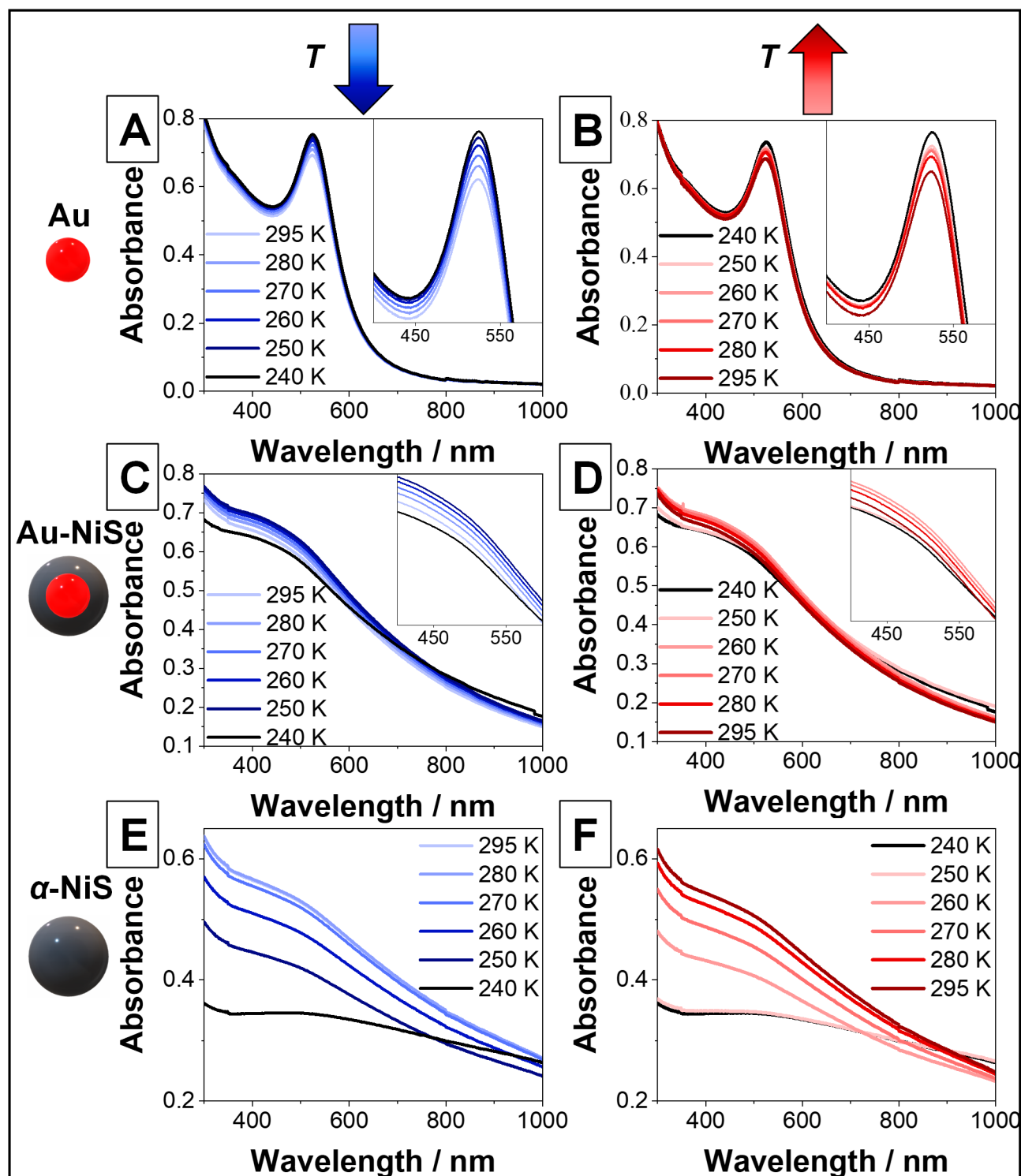


Figure 3. UV-vis absorbance spectra of (A,B) Au nanocrystals, diameter $6.1 \text{ nm} \pm 0.6 \text{ nm}$; (C,D) Au-NiS core-shell particles, diameter $15.2 \text{ nm} \pm 1.5 \text{ nm}$; and (E,F) α -NiS nanoparticles, diameter $16.8 \text{ nm} \pm 1.8 \text{ nm}$ at different temperatures. The panels on the left show the evolution of the spectra while the samples are cooled down, while on the right, the absorbance during the reheating of the nanoparticle solutions is observed.

particles of a similar diameter compared to the core-shell structures ($16.8 \text{ nm} \pm 1.8$ and $15.2 \text{ nm} \pm 1.5 \text{ nm}$, respectively), a different temperature dependence of the spectra is observed (Figure 3E,F). At room temperature, the LSPR, which is very similar to that of the Au-NiS particles, shows a broad absorbance shoulder reaching into the UV regime. It drops in intensity when the sample is cooled. Here, the change is a lot larger than the usual temperature dependence of an LSPR,

which can be seen by comparing the spectra to the respective ones of Au and Au-NiS nanocrystals. This trend continues until temperatures below 250 K are reached and no further change is observable. Yet, at these temperatures, the behavior of the LSPR is similar to the one of the core-shell particles since the pure nanoparticles also show a hysteresis where the 250 K spectrum during the reheating is identical to the 240 K spectrum. Also, in this case, if the temperature is raised even

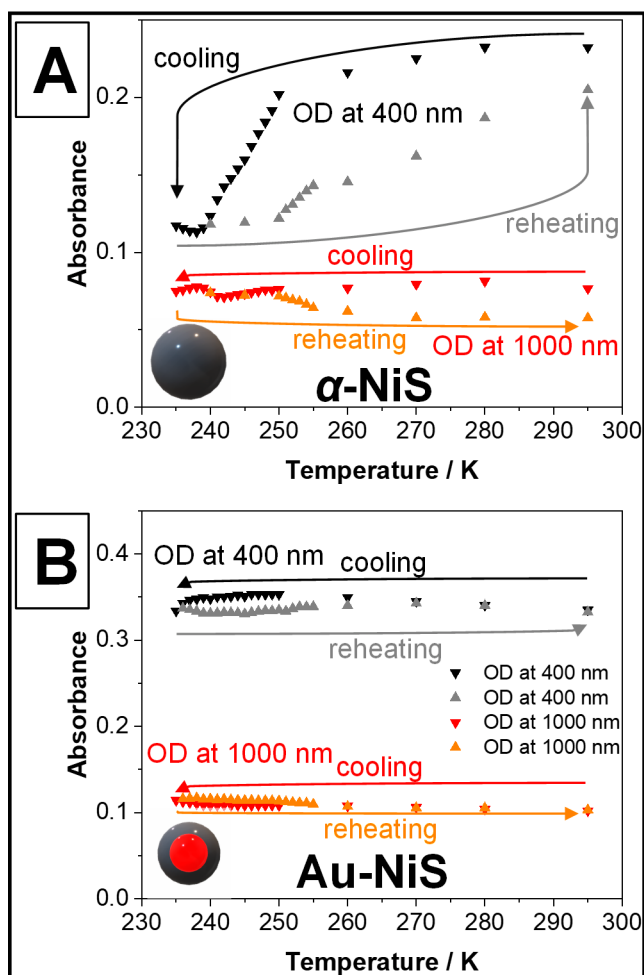


Figure 4. Optical density (OD) of dispersions of pure α -NiS nanoparticles (A) and Au-NiS core-shell particles (B) at 400 and 1000 nm during the cooling and reheating of the respective samples. It can be seen that during cooling, the OD at 400 nm decreases drastically in the case of the pure particles. The process seems to be reversible and also shows a hysteresis. For the Au-NiS particles, this hysteresis also exists but the OD does not drop (it increases instead) until a temperature below 245 K is reached. In both cases, the OD at 1000 nm increases at lower temperatures while also displaying a hysteresis. 235 K was the lowest achievable temperature with the used setup limited by the used solvent toluene.

further, the LSPR band is almost completely regained. It is possible that waiting for a longer time and measuring again would lead to a full recovery of the spectrum. Alternatively, it is also possible that a small part of the sample precipitated during the cooling and subsequent reheating processes, which each took several hours, and was therefore permanently removed from the optical path in the spectrometer resulting in the reduced absorbance at 295 K. Either way, the optical density of the pure α -NiS sample is apparently strongly and reversibly tunable in this manner.

To shine further light on the development of the spectra at lower temperatures, Figure 4 shows the absorbance of α -NiS and Au-NiS particles (equivalent to the respective samples displayed in Figure 3) at 400 and 1000 nm measured for a larger number of temperatures. It is obvious that the optical density (OD) of α -NiS at a wavelength of 400 nm drops significantly faster at temperatures below 250 K than above until a minimum is reached at about 240 K. The OD at 1000

nm also decreases at first, but once 242 K are reached it starts to increase again slightly. This leads to the conclusion that the phase transition of α -NiS starts at 250 K and is completed at around 240 K. Since the metallic character of the material is drastically reduced with the transition, the LSPR vanishes. If the low-temperature phase of α -NiS, which can be characterized as a very poorly conducting metal,² still displays an LSPR, it could theoretically be expected to appear deep in the IR part of the electromagnetic spectrum between wavelengths of 2000 and 10000 nm due to its low free charge carrier density of 10^{20} – 10^{21} /cm³.¹⁹ However, the investigation of these wavelengths was unfortunately not possible with the setup used in this work.

The determined temperature range for the transition could be due to the size distribution of the particles or different amounts of defects present in the particles (presumably due to a small Ni deficit). Generally, the reason why the transition temperature is slightly lower than in the bulk material (265 K) is the larger amount of defects present in the nanocrystals, which by their nature have a large surface-to-volume ratio where surface atoms can be treated as defects too. According to the literature, a transition temperature between 240 and 250 K would still correspond to a composition of Ni_{0.99}S or an even smaller Ni deficit.²⁰ At both investigated wavelengths, the change of the absorbance starts to turn back once a temperature of 250 K is reached during the reheating of the sample, which likely means the phase transition is being reversed as well. The decrease in absorbance accompanying a decreasing temperature above 250 K should therefore be caused by something else (see the discussion of the magnetic susceptibility measurements).

In the case of the Au-NiS core-shell particles, the absorbance at 400 nm rises with decreasing temperature until a temperature of 245 K is reached and it starts to drop. Along with this change, the absorbance at 1000 nm starts to increase. Both processes are only reversed once a temperature of 250 K is reached during the reheating of the sample. Above 260 K, the optical densities at both wavelengths are completely identical to the ones measured during the cooling of the particle dispersion. The change is therefore 100% reversible.

Thus, it can be assumed that both particle types show a phase transition at 240–250 K displaying a slight hysteresis between the values determined by the cooling and reheating steps of the experiment. The difference in the total decrease of the LSPR signal compared to the pure α -NiS particles could partly be explained by the remaining charge carrier density provided by the gold cores of the Au-NiS core-shell nanoparticles.

It has been shown for bulk α -NiS that the metal-insulator transition at $T_c \approx 265$ K is attended by a sharp magnetic phase transition from an (itinerant-electron) antiferromagnet below and a Pauli-paramagnetic metal above T_c , indicated by the observation of a small and only slightly temperature-dependent magnetic susceptibility in both regimes.^{20,21} Therefore, to further characterize the physical and optical properties of the different α -NiS systems, complementary magnetic susceptibility measurements were conducted at temperatures between $T = 4$ and 300 K with an external magnetic field of $H_{\text{ext}} = 1$ kOe. The syntheses of the samples used for these magnetic measurements were identical as for the samples used for the optical spectroscopy (*vide supra*); however, the syntheses had to be scaled up 7–10 times (for a full characterization of the thusly obtained particles, see Figure S4 in the Supporting

Information). In contrast to the bulk α -NiS material, the magnetic susceptibility of the α -NiS and Au-NiS nanoparticles studied here revealed a Curie-like temperature dependence (see Figure 5), suggesting that the magnetic susceptibility is

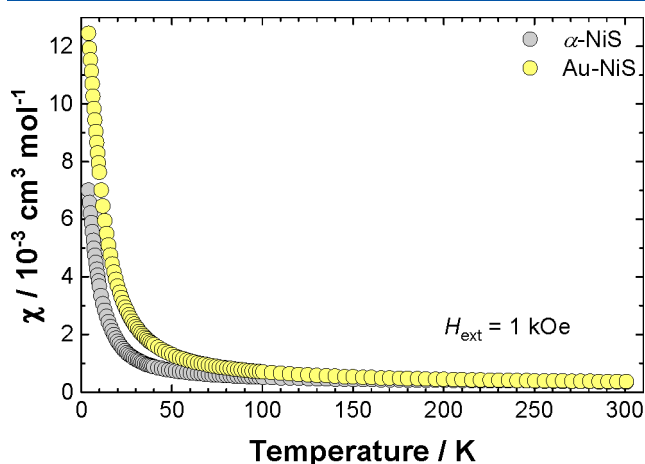


Figure 5. Molar magnetic susceptibility versus temperature of α -NiS (gray symbols) and Au-NiS (yellow symbols) nanoparticles recorded between $T = 4$ and 300 K with an external magnetic field of $H_{\text{ext}} = 1$ kOe. The measurements were conducted with a field warming sequence after zero-field cooling.

now predominantly related to a paramagnetic contribution. This qualitative result, and in particular the collapse of the antiferromagnetically long-range ordered state, is in accord with similar measurements on other nanoscale α -NiS systems where no antiferromagnetically long-range ordered state was achieved, and predominant paramagnetic contributions to the magnetic susceptibility were observed.^{22–24}

However, it should be noted here that the measurement of the magnetic susceptibility is an integral measurement of the magnetization of a macroscopic sample, and hence, it cannot be safely ruled out that for parts of the sample an antiferromagnetically ordered state is also formed but superimposed by a larger and strongly temperature-dependent paramagnetic contribution. Therefore, to further confirm the presence of predominating paramagnetic contributions on the magnetic susceptibility, supplementary isothermal magnetization measurements on α -NiS were conducted at temperatures of $T = 50, 235,$ and 300 K (cf. Figure S5 in the Supporting Information), consistently exhibiting a decreasing magnetic susceptibility ($\chi = \partial M / \partial H$) with increasing temperature. Contrarily, for an antiferromagnetically long-range ordered state (with external magnetic fields below the spin-flip transition), an increasing $\partial M / \partial H$ progression with rising temperature would be expected, while the Pauli spin-susceptibility is temperature independent in first order.

For a qualitative discussion of the magnetic properties of the α -NiS and Au-NiS nanoparticles, the temperature-dependent effective magnetic moment (μ_{eff}) per Ni atom was determined (using a simple Curie approximation with $\mu_{\text{eff}} \sim \sqrt{\chi T}$) and plotted in Figure 6. The displayed measurements were conducted starting at $T = 4$ K with a field-warming sequence after field or zero-field cooling to the base temperature, respectively.

Both compounds show similar behavior. Compared with the spin-only value of $\mu_{\text{eff}} = 2.83\mu_{\text{B}}$ (which is expected for a single ion $S = 1, \text{Ni}(2+), 3d^8$ paramagnetic high-spin center), the

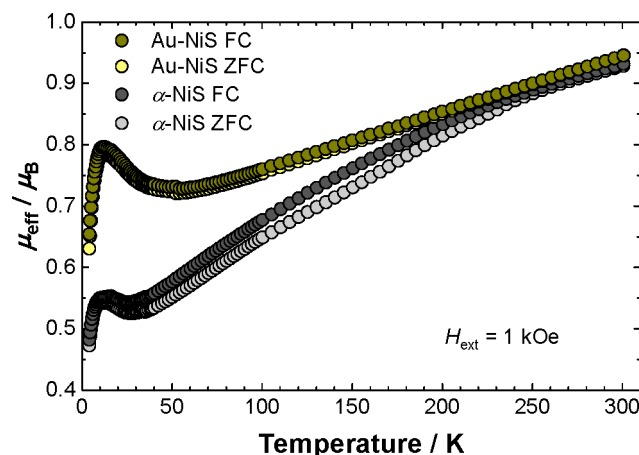


Figure 6. Effective magnetic moment (per Ni atom) versus temperature of α -NiS and Au-NiS nanoparticles recorded between $T = 4$ and 300 K with an external magnetic field of $H_{\text{ext}} = 1$ kOe. The measurements were conducted with a field warming sequence after field cooling (FC, dark gray and dark yellow symbols) or zero-field cooling (ZFC, gray and yellow symbols), respectively.

effective magnetic moment at $T = 300$ K of $\mu_{\text{eff}} \approx 0.94\mu_{\text{B}}$ per Ni atom is considerably reduced, indicating that strong antiferromagnetic (AF) correlations are still acting between an unknown number of (paramagnetic) Ni centers. These AF correlations are attributed to the strong AF ($<90^\circ$) super-exchange interaction along the c -axis of hexagonal α -NiS, which was also discussed to explain the magnetic structure of the antiferromagnetically long-range ordered state in the bulk α -NiS material.^{2,21} Consistently, a declining effective magnetic moment with decreasing temperature is observed for both investigated compounds; however, the progression with temperature is more pronounced for α -NiS, leading to a low-temperature ($T \rightarrow 0$) value for Au-NiS of $\sim 0.7\mu_{\text{B}}$ and for α -NiS of $\sim 0.5\mu_{\text{B}}$. Regarding the larger surface-to-volume ratio for the Au-NiS nanoparticles, it can be speculated that uncompensated magnetic (Ni) moments located in the (surface) shell of the nanoparticles are the source of this (temperature-independent) paramagnetic moment, while the magnetic moments that are located deeper in the shell (or in the core volume of pure α -NiS) exhibit stronger AF correlations and do not contribute to the magnetic susceptibility at low temperatures ($T \rightarrow 0$).

Another difference between both investigated α -NiS systems is visible in the field cooled (FC) and zero-field cooled (ZFC) measurements. While for Au-NiS particles (that carry a gold core), both curves are superimposed, the FC and ZFC curves markedly differ for pure α -NiS below $T \approx 250$ K, suggesting the presence of uncompensated magnetic moments that are located in the core volume of the α -NiS nanoparticles. To find further experimental evidence, the magnetic susceptibility measurements on α -NiS and Au-NiS particles were repeated with a larger external magnetic field of $H_{\text{ext}} = 5$ kOe. The results are shown in Figure S6 in the Supporting Information and revealed only a weak magnetic field dependence for the FC and ZFC curves (i.e., $\mu_{\text{eff}}^{\text{FC}} - \mu_{\text{eff}}^{\text{ZFC}} \approx \text{constant}$ for $H_{\text{ext}} = 1$ and 5 kOe), indicating that a magnetic field-induced spin canting effect can be ruled out as the major source for the different FC and ZFC behavior of α -NiS and Au-NiS. However, a spin canting due to magnetic anisotropy²⁵ and, alternatively, interparticle interactions²³ may also contribute to thermal

hysteresis effects, but unfortunately a reliable conclusion appears not yet possible based on the available data.

Finally, at low temperatures ($T \approx 10$ K), a distinct maximum of the temperature-dependent effective magnetic moment is observed for both investigated materials, indicating that ferromagnetic (FM) correlations become relevant at these temperatures. Again, regarding the magnetic structure of hexagonal bulk α -NiS, the increasing low-temperature magnetic susceptibility can be attributed to the weak ferromagnetic (nearly 90°) superexchange interaction along the ab -plane of α -NiS (leading to the ferromagnetic alignment of Ni atoms within the ab -plane of bulk α -NiS).² Alternatively, a similar “low-temperature anomaly” was also reported for the magnetic susceptibility of other nanoscale α -NiS systems, and spin-frustration (or a spin-glass phase) associated with uncompensated magnetic moments located in the surface shell of the nanoparticles²³ and/or superparamagnetic blocking behavior together with a considerable magnetic field hysteresis^{23,24} were discussed. The isothermal magnetization measurements of α -NiS and Au-NiS nanoparticles recorded at $T = 4$ K are shown in Figure S7 in the Supporting Information, revealing that for α -NiS a clearly resolved hysteresis is not achieved. However, indications of a small FM contribution can be anticipated and in particular also for the isothermal magnetization at an elevated temperature of $T = 300$ K (cf. Figure S5 in the Supporting Information). Together with a considerable magnetic field dependence of the effective magnetic moment of α -NiS (cf. Figure S6 in the Supporting Information), this anticipated FM contribution is probably associated with a small ferromagnetic impurity (presumably Ni metal) and not with the α -NiS nanoparticles. For the Au-NiS sample, the isothermal magnetization at $T = 300$ K exhibits the expected (paramagnetic) linear $M(H)$ progression (cf. Figure S5 in the Supporting Information), while at $T = 4$ K a small magnetic field hysteresis (with a low coercivity field of ~ 185 Oe) is found, which is in accord with similar measurements on other nanoscale α -NiS systems.^{22–24}

In conclusion, the magnetic susceptibility of the investigated compounds revealed some similarities, i.e., (1) a Curie-like magnetic susceptibility (suggesting the presence of uncompensated magnetic moments in these materials), (2) the presence of AF correlations that are observed over the full temperature range, and (3) a low-temperature anomaly (at $T \approx 10$ K) that is attributed to weak FM correlations or spin-frustration. Some differences are also obvious, i.e., (1) a marked discrepancy of the field and zero-field cooled temperature-dependent magnetic susceptibility, which is relevant only for the α -NiS compound (suggesting that uncompensated magnetic moments in the core volume of the nanoparticles are involved), (2) a larger value of the magnetic susceptibility in the low-temperature limit ($T \rightarrow 0$) for Au-NiS, indicating a larger number of uncompensated magnetic moments located in the surface shell of Au-NiS than for α -NiS nanoparticles, and (3) a small magnetic field hysteresis that was observed for Au-NiS at $T = 4$ K, while a clearly resolved hysteresis was not achieved at the same temperature for α -NiS. Since the spectroscopic measurements revealed a significant change of the optical properties at characteristic temperatures between $T = 240$ and 250 K associated with a metal–insulator-like transition, the investigation of the magnetic properties was insofar surprising that the magnetic susceptibility revealed a paramagnetic regime in first order without a distinct anomaly in the relevant temperature range. However, assuming that the presence of

uncompensated magnetic moments, and in the case of α -NiS presumably those that are located in the core volume of the individual nanoparticles, also impairs the mobility of the free charge carriers and therefore the intensity of the LSPR, it could possibly explain the decline of the optical absorbance spectra of the α -NiS particles above their (optical) transition temperature.

CONCLUSIONS

Synthesis procedures to obtain monodisperse α -NiS and Au-NiS core–shell nanoparticles, which show an LSPR in the visible regime of the electromagnetic spectrum, were developed. When the particles are cooled down to 240 – 250 K, a reversible change to the optical spectra, likely associated with the phase transition of α -NiS, is triggered. In the case of the pure nickel sulfide, there is an additional effect which, according to the measurements of the magnetic susceptibility, could be due to the presence of uncompensated magnetic moments that are presumably located in the core volume of the individual nanoparticles. Here, the observed change in optical density is quite drastic making this an interesting switchable material for various plasmonic applications (e.g., fluorescence enhancement applications or sensory applications). In the future, the temperature of the transition could be raised (possibly even above room temperature) or decreased in accordance with the specific demands of an application by doping the α -NiS with other metals like iron or cobalt, respectively.²⁶

ASSOCIATED CONTENT

Supporting Information

The Supporting Information is available free of charge at <https://pubs.acs.org/doi/10.1021/acs.jpcc.1c08412>.

TEM analysis and UV–vis absorbance spectra of AuNCs, XRD and UV–vis analysis of Au-NiS core–shell nanoparticles, full characterization of particles obtained by upscaled syntheses, and magnetic susceptibility measurements on α -NiS and Au-NiS nanoparticles (PDF)

AUTHOR INFORMATION

Corresponding Author

Dirk Dorfs – Institute of Physical Chemistry and Electrochemistry, Leibniz Universität Hannover, 30167 Hannover, Germany; Laboratory of Nano and Quantum Engineering, Leibniz Universität Hannover, 30167 Hannover, Germany; Cluster of Excellence PhoenixD (Photonics, Optics, and Engineering–Innovation Across Disciplines), Leibniz Universität Hannover, 30167 Hannover, Germany; orcid.org/0000-0001-6175-4891; Email: dirk.dorfs@pci.uni-hannover.de

Authors

Rasmus Himstedt – Institute of Physical Chemistry and Electrochemistry, Leibniz Universität Hannover, 30167 Hannover, Germany; Laboratory of Nano and Quantum Engineering, Leibniz Universität Hannover, 30167 Hannover, Germany; orcid.org/0000-0003-0793-5258

Dirk Baabe – Institut für Anorganische und Analytische Chemie, Technische Universität Braunschweig, 38106 Braunschweig, Germany

Christoph Wesemann – Institute of Physical Chemistry and Electrochemistry, Leibniz Universität Hannover, 30167 Hannover, Germany; Laboratory of Nano and Quantum Engineering, Leibniz Universität Hannover, 30167 Hannover, Germany; orcid.org/0000-0003-1240-7257

Patrick Bessel – Institute of Physical Chemistry and Electrochemistry, Leibniz Universität Hannover, 30167 Hannover, Germany; Laboratory of Nano and Quantum Engineering, Leibniz Universität Hannover, 30167 Hannover, Germany; orcid.org/0000-0002-8658-6190

Dominik Hinrichs – Institute of Physical Chemistry and Electrochemistry, Leibniz Universität Hannover, 30167 Hannover, Germany; Laboratory of Nano and Quantum Engineering, Leibniz Universität Hannover, 30167 Hannover, Germany

Anja Schlosser – Institute of Physical Chemistry and Electrochemistry, Leibniz Universität Hannover, 30167 Hannover, Germany; Laboratory of Nano and Quantum Engineering, Leibniz Universität Hannover, 30167 Hannover, Germany; orcid.org/0000-0001-9669-8383

Nadja C. Bigall – Institute of Physical Chemistry and Electrochemistry, Leibniz Universität Hannover, 30167 Hannover, Germany; Laboratory of Nano and Quantum Engineering, Leibniz Universität Hannover, 30167 Hannover, Germany; Cluster of Excellence PhoenixD (Photonics, Optics, and Engineering–Innovation Across Disciplines), Leibniz Universität Hannover, 30167 Hannover, Germany; orcid.org/0000-0003-0171-1106

Complete contact information is available at:
<https://pubs.acs.org/10.1021/acs.jpcc.1c08412>

Notes

The authors declare no competing financial interest.

ACKNOWLEDGMENTS

D.D. and N.C.B. are thankful for funding by the German Research Foundation (DFG Research Grants DO 1580/5-1 and BI 1708/4-1, respectively). D.D. and N.C.B. also acknowledge financial support by the DFG under Germany's Excellence Strategy within the Cluster of Excellence PhoenixD (EXC 2122, Project ID 390833453). R.H., P.B., and A.S. are grateful for being funded by the Hannover School for Nanotechnology (HSN). D.B. thanks Martin Bröring (Institut für Anorganische und Analytische Chemie at TU Braunschweig) for providing the SQUID magnetometer. N.C.B. and A.S. furthermore received funding from the European Research Council (ERC) under the European Union's Horizon 2020 Research and Innovation Program (Grant Agreement No. 714429). The authors would also like to thank Tim Göpfert and Max Niemeyer for preliminary work leading up to this study and Armin Feldhoff as well as Jürgen Caro for the possibility to use the XRD.

REFERENCES

- (1) White, R. M.; Mott, N. F. The Metal-Non-Metal Transition in Nickel Sulphide (NiS). *Philos. Mag.* **1971**, *24*, 845–856.
- (2) Panda, S. K.; Dasgupta, I.; Sastoglu, E.; Blugel, S.; Sarma, D. D. NiS - An Unusual Self-Doped, Nearly Compensated Antiferromagnetic Metal. *Sci. Rep.* **2013**, *3*, 2995.
- (3) Trahan, J.; Goodrich, R. G. Heat Capacity of Hexagonal NiS: Metal-Nonmetal Transition. *Phys. Rev. B* **1972**, *6*, 199–203.
- (4) Mott, N. F. *Metal-Insulator Transitions*, 2nd ed.; CRC Press: London, 1990.

(5) Himstedt, R.; Rusch, P.; Hinrichs, D.; Kodanek, T.; Lauth, J.; Kinge, S.; Siebbeles, L. D. A.; Dorfs, D. Localized Surface Plasmon Resonances of Various Nickel Sulfide Nanostructures and Au-Ni₃S₂ Core-Shell Nanoparticles. *Chem. Mater.* **2017**, *29*, 7371–7377.

(6) Okamura, H.; Naitoh, J.; Nanba, T.; Matoba, M.; Nishioka, M.; Anzai, S.; Shimoyama, I.; Fukui, K.; Miura, H.; Nakagawa, H.; et al. Optical Study of the Metal–Nonmetal Transition in NiS. *Solid State Commun.* **1999**, *112*, 91–95.

(7) Bercea, A. I.; Champeaux, C.; Constantinescu, C. D.; Dumas-Bouchiat, F. Vanadium Dioxide–Iridium Composite Development: Specific Near Infrared Surface Plasmon Resonance. *J. Compos. Sci.* **2021**, *5*, 193.

(8) Ke, Y.; Zhang, B.; Wang, T.; Zhong, Y.; Vu, T. D.; Wang, S.; Liu, Y.; Magdassi, S.; Ye, X.; Zhao, D.; et al. Manipulating Atomic Defects in Plasmonic Vanadium Dioxide for Superior Solar and Thermal Management. *Mater. Horiz.* **2021**, *8*, 1700–1710.

(9) Nishikawa, K.; Kishida, Y.; Ito, K.; Tamura, S.; Takeda, Y. Near-Infrared Localized Surface Plasmon Resonance of Self-Growing W-Doped VO₂ Nanoparticles at Room Temperature. *Appl. Phys. Lett.* **2017**, *111*, 193102.

(10) Savant, V. V.; Gopalakrishnan, J.; Patel, C. C. Studies on Some Metal Monothiobenzoates. *Inorg. Chem.* **1970**, *9*, 748–751.

(11) Tat, K. W. *Design and Characterization of Some Novel Magnetic Nanomaterials*. Ph.D. Dissertation, National University of Singapore, Singapore, 2007.

(12) Peng, S.; Lee, Y.; Wang, C.; Yin, H.; Dai, S.; Sun, S. A Facile Synthesis of Monodisperse Au Nanoparticles and Their Catalysis of CO Oxidation. *Nano Res.* **2008**, *1*, 229–234.

(13) Zhu, W.; Michalsky, R.; Metin, Ö.; Lv, H.; Guo, S.; Wright, C. J.; Sun, X.; Peterson, A. A.; Sun, S. Monodisperse Au Nanoparticles for Selective Electrocatalytic Reduction of CO₂ to CO. *J. Am. Chem. Soc.* **2013**, *135*, 16833–16836.

(14) Bain, G. A.; Berry, J. F. Diamagnetic Corrections and Pascal's Constants. *J. Chem. Educ.* **2008**, *85*, 532–536.

(15) Himstedt, R.; Hinrichs, D.; Dorfs, D. Extinction Coefficient of Plasmonic Nickel Sulfide Nanocrystals and Gold-Nickel Sulfide Core-Shell Nanoparticles. *Z. Phys. Chem.* **2018**, *233*, 3–14.

(16) Rodríguez-González, B.; Burrows, A.; Watanabe, M.; Kiely, C. J.; Liz Marzán, L. M. Multishell Bimetallic AuAg Nanoparticles: Synthesis, Structure and Optical Properties. *J. Mater. Chem.* **2005**, *15*, 1755–1759.

(17) Himstedt, R.; Hinrichs, D.; Sann, J.; Weller, A.; Steinhauser, G.; Dorfs, D. Halide Ion Influence on the Formation of Nickel Nanoparticles and Their Conversion into Hollow Nickel Phosphide and Sulphide Nanocrystals. *Nanoscale* **2019**, *11*, 15104–15111.

(18) Yeshchenko, O. A.; Bondarchuk, I. S.; Gurin, V. S.; Dmitruk, I. M.; Kotko, A. V. Temperature Dependence of the Surface Plasmon Resonance in Gold Nanoparticles. *Surf. Sci.* **2013**, *608*, 275–281.

(19) Luther, J. M.; Jain, P. K.; Ewers, T.; Alivisatos, A. P. Localized Surface Plasmon Resonances Arising from Free Carriers in Doped Quantum Dots. *Nat. Mater.* **2011**, *10*, 361–366.

(20) Sparks, J. T.; Komoto, T. Metal-to-Semiconductor Transition in Hexagonal NiS. *Rev. Mod. Phys.* **1968**, *40*, 752–754.

(21) Coey, J. M. D.; Brusetti, R.; Kallel, A.; Schweizer, J.; Fuess, H. Nickel Sulfide—an Itinerant-Electron Antiferromagnet. *Phys. Rev. Lett.* **1974**, *32*, 1257–1260.

(22) Zhang, H. T.; Wu, G.; Chen, X. H. Synthesis and Magnetic Properties of NiS_{1+x} Nanocrystallines. *Mater. Lett.* **2005**, *59*, 3728–3731.

(23) Barry, L.; Holmes, J. D.; Otway, D. J.; Copley, M. P.; Kazakova, O.; Morris, M. A. Unusual Magnetism in Templated NiS Nanoparticles. *J. Phys.: Condens. Matter* **2010**, *22*, 076001.

(24) Tang, C.; Zang, C.; Su, J.; Zhang, D.; Li, G.; Zhang, Y.; Yu, K. Structure and Magnetic Properties of Flower-like α -NiS Nanostructures. *Appl. Surf. Sci.* **2011**, *257*, 3388–3391.

(25) Carlin, R. L. *Magnetochemistry*; Springer Berlin Heidelberg: Berlin, Heidelberg, Germany, 1986.

(26) Nakamura, M.; Fujimori, A.; Sacchi, M.; Fuggle, J. C.; Misu, A.; Mamori, T.; Tamura, H.; Matoba, M.; Anzai, S. Metal-Nonmetal

Transition in NiS Induced by Fe and Co Substitution: X-Ray-Absorption Spectroscopic Study. *Phys. Rev. B: Condens. Matter Mater. Phys.* **1993**, *48*, 16942–16947.